Effect of Barium Loading on the Desulfation of Pt-BaO/Al_2O_3 Studied by H_2 TPRX, TEM, Sulfur K-edge XANES, and in Situ TR-XRD

Do Heui Kim,*,† Janos Szanyi,† Ja Hun Kwak,† Tamas Szailer,† Jonathan Hanson,‡ Chong Min Wang,† and Charles H. F. Peden†

Institute for Interfacial Catalysis, Pacific Northwest National Laboratory, Richland, Washington 99352, and Chemistry Department, Brookhaven National Laboratory, Upton, New York 11973

Received: January 6, 2006; In Final Form: March 21, 2006

Desulfation processes were investigated over sulfated Pt-BaO/Al_2O_3 with different barium loading (8 and 20 wt %) by using H_2 temperature programmed reaction (TPRX), transmission electron microscope (TEM) with energy dispersive spectroscopy (EDS), sulfur K-edge X-ray absorption near-edge spectroscopy (XANES), and in situ time-resolved X-ray diffraction (TR-XRD) techniques. Both sulfated samples (8 and 20 wt %) form sulfate species (primarily $BaSO_4$) as evidenced by S K-edge XANES and in situ TR-XRD. However, the desulfation behavior is strongly dependent on the barium loading. Sulfated Pt-BaO(8)/Al_2O_3, consisting predominantly of surface BaO/$BaCO_3$ species, displays more facile desulfation by H_2 at lower temperatures than sulfated Pt-BaO(20)/Al_2O_3, a material containing primarily bulk BaO/$BaCO_3$ species. Therefore, after desulfation with H_2 up to 1073 K, the amount of the remaining sulfur species on the former, mostly as BaS, is much less than that on the latter. This suggests that the initial morphology differences between the two samples play a crucial role in determining the extent of desulfation and the temperature at which it occurs. It is concluded that the removal of sulfur is significantly easier at lower barium loading. This finding can potentially be important in developing more sulfur resistant LNT catalyst systems.

1. Introduction

The lean NOx trap (LNT) technology,[1] also known as NOx adsorber and NOx storage/reduction catalysts, is considered as one of the promising solutions to reduce NOx emissions from lean burn engines. Typically, the LNT catalyst, which consists of precious metal (e.g., Pt), a storage material (alkali and/or alkaline earth oxides; e.g., BaO), and a high surface support material (e.g., Al_2O_3), operates under transient conditions.[2] During a lean cycle, NO is oxidized to NO_2 over Pt sites and the NO_2 reacts with BaO/$BaCO_3$ species to form $Ba(NO_3)_2$. After barium sites are saturated with nitrate species, reductants such as H_2, CO, or hydrocarbons (sometimes, the fuel itself) are introduced for a short rich period. The stored NOx is released and reduced over Pt (and other precious metal) sites with the reductants. Although continuing research regarding NOx storage and regeneration steps is providing for a good understanding of LNT performance,[3−11] the stability of the material against SO_2 poisoning remains a critical issue.

As with NO, SO_2 is oxidized to SO_3 over Pt sites. Thus, the LNT catalyst is poisoned by SO_2 due to the higher affinity of the barium sites for SO_3 than NO_2 because $BaSO_4$ is thermodynamically more stable than BaO or $Ba(NO_3)_2$.[9] Formation of $BaSO_4$ gives rise to a decrease in the available sites for NOx adsorption, correspondingly leading to the deactivation of the catalyst. Even low concentrations of SO_2 gradually reduce the ability for the NOx storage, and it has been shown that the degree of deactivation of NOx storage capacity is approximately proportional to the total SO_2 dose.[12] Desulfation of the LNT material (essentially decomposition and/or reduction of $BaSO_4$) requires high temperatures (e.g., 873 K and higher) leading to irreversible deactivation via Pt sintering and/or $BaAl_2O_4$ formation from a solid-state reaction between the Ba phase and alumina.[1]

Two types of barium sulfates in Pt/BaO/Al_2O_3 LNT catalysts have been identified based primarily on IR spectroscopy: surface and bulk sulfates.[13−15] It has been suggested that as the sulfation proceeds the surface sulfates on barium are slowly converted to bulk sulfates, which are more stable against reduction.[15] Similarly, previous H_2 temperature-programmed reduction (TPRX) studies[16,17] have suggested that H_2S features near 673−773 K can be attributed to the desulfation of aluminum sulfate while those above 873 K are due to surface and bulk barium sulfate species.

We have shown that the NOx adsorption/desorption chemistry is dependent on the loading of barium.[6,18] NO_2 adsorption at 573 K on 8 wt % BaO/Al_2O_3 generates mostly surface barium nitrates that coat and nearly completely cover the alumina surface, while bulklike barium nitrates are dominant on a 20 wt % BaO/Al_2O_3 sample. These assignments were based on IR, ^{15}N NMR, XRD, TEM, and TPD results, and we found it especially important to use multiple techniques and materials with a wide range of Ba loadings in making these assignments. We should note that, to our knowledge, there has not been an analogous thorough study performed to date for SOx adsorption and reaction; notably one that directly correlated H_2 TPRX data with results from IR spectroscopy for model LNT materials with various Ba loadings.

Still, considering the likely presence of multiple morphologies for sulfate and nitrate Ba phases, an important question to ask concerns how the desulfation chemistry depends on these morphology differences arising from the different barium loadings. Understanding the desulfation chemistry will be helpful

* Address correspondence to this author. E-mail: do.kim@pnl.gov.
† Pacific Northwest National Laboratory.
‡ Brookhaven National Laboratory.

10.1021/jp060119f CCC: $33.50
Published on Web 05/05/2006

to develop more durable LNT catalysts with less deactivation by SO_2 and/or more facile regeneration. Thus, the purpose of the study reported here was to investigate desulfation processes for sulfated Pt-BaO/Al_2O_3 materials with varying barium loading by applying H_2 temperature programmed reaction (TPRX), transmission electron microscope (TEM) with energy dispersive spectroscopy (EDS), sulfur K-edge XANES (X-ray near-edge spectroscopy), and in situ TR-XRD (time-resolved X-ray diffraction) techniques.

2. Experimental Section

The 8 and 20 wt % BaO/Al_2O_3 samples were prepared by the incipient wetness method, using an aqueous $Ba(NO_3)_2$ solution, followed by drying in an oven at 393 K. Multiple incipient wetness steps were performed to reach the desired Ba loading. The γ-Al_2O_3 (Condea) used as the support for catalyst preparation had a surface area of 200 m^2/g. Pt was impregnated onto $Ba(NO_3)_2/Al_2O_3$ by the incipient wetness method, using an aqueous $Pt(NH_3)_4(NO_3)_2$ solution. The loading of Pt was 2 wt %. Following another drying step, this material was then subjected to a calcination process in flowing 5% O_2/He. For this, the furnace temperature was raised to 773 K at a rate of 1 deg/min and maintained at 773 K for 5 h. The two samples have similar Pt dispersions of ~45−50% as determined by H_2 chemisorption, and TEM also shows that the Pt particles size of two samples is essentially the same.

Before starting the sulfation process, the sample (0.15 g) was placed in a quartz reactor and treated with 10% O_2 in He at 773 K for an additional 2 h. Sulfation was performed at 573 K for 6 h in a gas mixture of 50 ppm of SO_2 and 10% O_2 balanced with helium (total flow rate: 150 cm^3/min), designated as 5 g/L sulfation. For the case of 10 g/L sulfation, all the conditions are the same except the doubled sulfation time (12 h). During the sulfation, SO_2 breakthrough was continuously monitored with a mass spectrometer (MKS, Minilab).

H_2 TPRX (temperature programmed reaction) experiments were performed for the sulfated samples in the same reactor by raising the temperature to 1073 K at a rate of 8 deg/min under flowing 20% H_2/He. The desorbed gases were detected with the same mass spectrometer. The samples obtained after H_2 TPRX experiment to 1073 K were designated as "desulfated". Additional samples were collected and stored in a glass vial with minimum air and moisture exposures after ramping the temperature up to 553 and 743 K in the H_2/He environment to use for the XANES experiment, providing a "snapshot" of the oxidation state of sulfur at various stages of the H_2 TPRX process.

The TR-XRD experiments and sulfur K-edge XANES were carried out at beam lines ×7B and ×19A of the National Synchrotron Light Source (NSLS) at Brookhaven National Laboratory, respectively. The detailed experimental setup of the TR-XRD has been described elsewhere.[19] A small amount of sulfated sample was placed in a sapphire tube and heated at 10 deg/min from 300 to 1073 K while continuously flowing a 5% H_2 in He gas mixture. XRD patterns were collected in situ every 2 min during the temperature ramping. The ×19A beamline used to collect the S K-edge XANES data is equipped with a double-crystal Si(111) monochromator. Ultrahigh vacuum (UHV) conditions (about 10^{-10} Torr) were maintained along the beampipe to the experimental hutch. Fluorescence measurements were performed with a passivated implanted planar silicon (PIPS) detector (Canberra Industries, CT). The beam path from the incident ion chamber to the sample chamber was purged with He gas. The well ground samples were evenly spread over a sulfur-free tape. After calibrating the X-ray energy for the K-edge of elemental sulfur (Aldrich), its peak position was assigned an energy value of 2472 eV and scans ranging from 20 eV below and to 50 eV above the absorption edge of S were collected for all subsequent samples with a step size of 0.5 eV. The resolution of all the data collected is about 0.5 eV. The reference materials ($BaSO_4$, BaS, and $Al_2(SO_4)_3$) were purchased from Aldrich

TABLE 1: Amount of SO_2 Uptake during Sulfation and H_2S Formation during H_2 TPRX up to 1073 K

	Ba (mmol)	SO_2 uptake (mmol)	H_2S desorbed (arb. units)
Pt-BaO(8)/Al_2O_3, 5 g/L sulfated	0.078	0.092	147
Pt-BaO(20)/Al_2O_3, 5 g/L sulfated	0.196	0.121	67
Pt-BaO(20)/Al_2O_3, 10 g/L sulfated	0.196	0.176	−

TEM images were collected from sulfated 5 g/L Pt(2)-BaO(8)/Al_2O_3 and Pt(2)-BaO(20)/Al_2O_3 samples, as well as desulfated 5 g/L Pt(2)-BaO(8)/Al_2O_3 and Pt(2)-BaO(20)/Al_2O_3 ones. The TEM specimens were prepared by dusting the powder particles onto a carbon film-coated 200 mesh copper TEM grid. TEM analysis was carried out on a JEOL JEM 2010 microscope with a specified point-to-point resolution of 0.194 nm. The operating voltage of the microscope was 200 keV. All images were digitally recorded with a slow scan CCD camera (image size 1024 × 1024 pixels), and image processing was carried out with a Digital Micrograph (Gatan). The composition of the particles was analyzed by energy-dispersive X-ray spectroscopy (EDS), using an Oxford Link spectrometer attached onto the transmission electron microscope.

3. Results

Table 1 summarizes the integral SO_2 uptake during the sulfation over Pt-BaO/Al_2O_3 with different barium loadings and sulfation levels. Although 5 g/L sulfation is applied to both samples, the amount of SO_2 uptake over Pt-BaO(20)/Al_2O_3 is much larger than that over the Pt-BaO(8)/Al_2O_3 sample, indicating that this SO_2 exposure level was sufficient to fully sulfate the Ba component of the latter material. In fact, Table 1 also indicates that the amount of SO_2 uptake over Pt-BaO(8)/Al_2O_3 exceeds what would be expected in the case of full conversion of BaO to $BaSO_4$. This result can be rationalized by the participation of the aluminum oxide in additional adsorption of SO_2, consistent with prior literature.[13−15] Our previous results[6] also provide evidence that a Pt-BaO(8)/Al_2O_3 sample still contains exposed alumina surface. In contrast, the alumina surface in the Pt-BaO(20)/Al_2O_3 sample should be essentially fully covered with BaO/$BaCO_3$ and contain "bulk" BaO/$BaCO_3$ phase since the amount of barium loading is more than a monolayer coverage. As presented in Table 1, in case of 10 g/L sulfation, the SO_2 uptake of Pt-BaO(20)/Al_2O_3 sample (0.176 mmol) was actually less than the amount of barium (0.196 mmol), although the total SO_2 introduced (0.242 mmol) is more that that of barium. Also as the sulfation proceeds, the SO_2 breakthrough occurred and the uptake of SO_2 became slower. Analogous to the diffusion limitations on the $Ba(NO_3)_2$ formation on large Ba-containing particles during the NOx uptake,[20] one might apply it to the sulfation process. Therefore, the limited sulfation over the sample with high barium loading at the higher SO_2 exposure can be explained by the diffusion limitations for SO_2/SO_3 into the core of the bulk BaO/$BaCO_3$ particles.

Figure 1 shows the H_2 TPRX spectra of 5 g/L sulfated Pt-BaO(8)/Al_2O_3 and Pt-BaO(20)/Al_2O_3 samples. H_2S is the

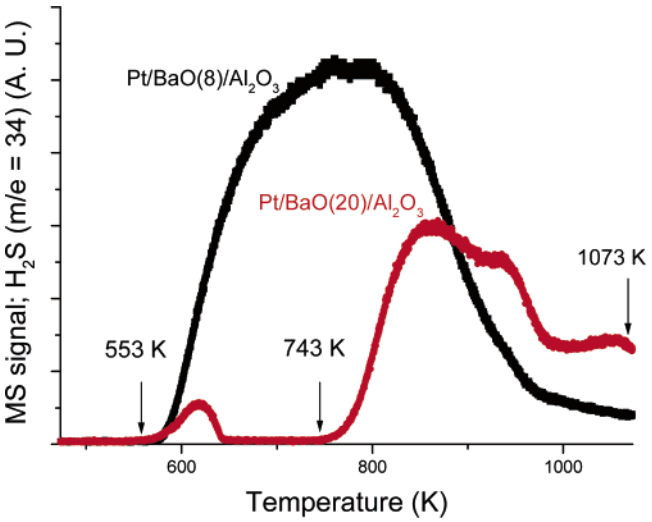

Figure 1. H_2 TPRX spectra for 5 g/L Pt-BaO(8)/Al_2O_3 and 5 g/L Pt-BaO(20)/Al_2O_3 samples.

primary product of the reaction between H_2 and sulfur species on the samples. Although SO_2 is also observed, the amount of SO_2 is no more than about one-tenth of H_2S desorption and the position of the SO_2 TPRX feature is overlapped with that of H_2S. Therefore, we have only included the H_2S features in the figure. Previous TPRX studies[16,17] have suggested that H_2S features near 673−773 K can be attributed to the desulfation of aluminum sulfate while those above 873 K are correspondingly due to surface and bulk barium sulfate species. In comparing this previous work to ours, it is important to keep in mind that the conditions of barium loading and the sulfation/desulfation methods are somewhat different from ours. Furthermore as noted above, we believe that definitive assignments should be made on the basis of a thorough study that directly correlates H_2 TPRX data with results from other spectroscopies (i.e., IR) for model LNT materials with various Ba loadings. Still, it is reasonable to conclude that the H_2S formation at higher temperature for the sample with higher Ba loadings (i.e., Pt-BaO(20)/Al_2O_3) results from the desulfation of more bulklike barium sulfate. Correspondingly, the lower temperature H_2S formation for the Pt-BaO(8)/Al_2O_3 sample suggests the formation of surface barium sulfates, and perhaps aluminum sulfate as well. Thus, the clear differences observed in the H_2 TPRX data for these two samples imply that the type of barium sulfate species formed upon uptake of SO_2 is different depending on the loading of barium species (surface or bulk), resulting in totally different desorption behavior. As another indication that sulfate morphology is playing a role in determining the ease of desulfation, Table 1 shows that the low loading of barium produces two times the amount of H_2S in the H_2 TPRX experiment than the sample with higher barium loading, even though the initial amount of SO_2 uptake over the low Ba-loaded sample is less. Thus, the removal of sulfur from the Pt-BaO(8)/Al_2O_3 sample occurs significantly more completely and at lower temperature.

Sulfur K-edge XANES experiments were carried out to investigate changes in the oxidation states of the sulfur as a function of H_2 reduction temperature. It has been found that the broad white line absorption spectrum, which arises from the S 1s to S 3p electronic transition, can be used to identify the major sulfur containing functional groups, such as sulfide, sulfite, and sulfate.[21−23] Moreover, Rodriguez et al.[24,25] demonstrated that the sulfur K-edge peak position increases proportionally with increasing sulfur oxidation states from −2 to +6. Figure 2 displays the S K-edge XANES spectra of a few reference materials. The position of the strong peak ("white line") in the spectra of $BaSO_4$ at 2482 eV indicates the presence of S^{6+} species. Despite the same oxidation state, the white line of $Al_2(SO_4)_3$ is located at 2483 eV. For the BaS reference sample, several peaks exist from 2472 to 2480 eV. The feature at 2472 eV can be assigned to the formally S^{2-} species in BaS. A previous study has demonstrated that contamination by sulfates leads to a peak at approximately 2480 eV for all sulfides except for an ultra dry one.[26] Although the XANES result in Figure 2 indicates that there are a variety of sulfur oxidation states in the BaS standard used here, the XRD pattern from this sample clearly shows the existence of only a BaS phase, implying that the species at energy higher than 2472 eV can be attributed to the small amount of surface sulfates or sulfites arising from the contamination of the moisture in the atmosphere.

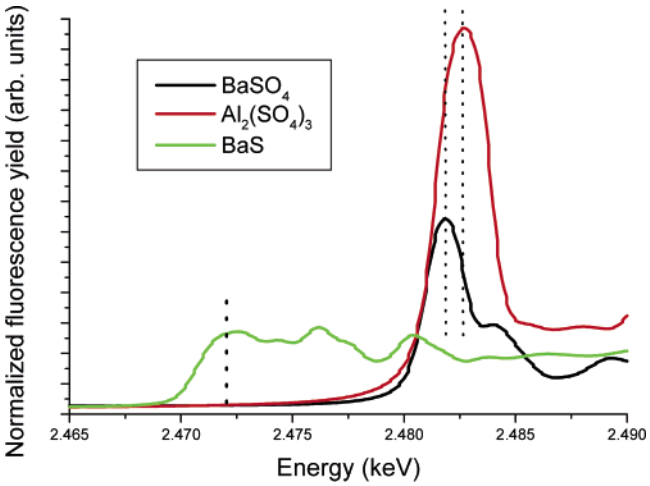

Figure 2. Sulfur K-edge spectra of reference samples.

We collected Pt-BaO(8)/Al_2O_3 and Pt-BaO(20)/Al_2O_3 samples after H_2 TPRX up to 553 and 1073 K, and 553, 743 and 1073 K, respectively. These specific reduction temperatures are identified in Figure 1 to qualitatively indicate the extent of sulfur removal from the various samples studied here. Figure 3 shows their sulfur XANES spectra. The spectra for both sulfated samples before reduction (black curves in Figure 3a,b) have a single peak at 2482 eV and a shoulder at 2484 eV, which can be assigned to barium sulfate species, not aluminum sulfate species, whose peak is located at 2483 eV. After H_2 TPRX up to 553 K for the Pt-BaO(8)/Al_2O_3 sample, the spectrum (Figure 3a, red curve) contains a small peak at 2472 eV, which can be assigned to a sulfide-like (S^{2-}) species based on BaS reference in Figure 2, along with a very small reduction in the sulfate peak. This demonstrates that the even at a low H_2 reduction temperature (553 K), below which no gaseous H_2S is formed, a small amount of sulfide is formed at the expense of sulfate species. After H_2 TPRX up to 1073 K, the sulfate peaks nearly disappear, while there is an increase in features from lower oxidation state sulfur species due to sulfide-like (2472 eV, S^{2-}) and sulfite-like (2478 eV, SO_3^{2-}) species. It should be noted that the intensity of these peaks depends strongly on the occupany of the S p states, and therefore, the intensities of the feature with different oxidation states (S^{6+} and S^{2-}) cannot be directly compared.[27] Song et al.[26] reported that the pure sulfates show roughly 5 times the absorption intensities of the pure sulfides. This implies that the species remaining after H_2 TPRX up to 1073 K are primarily sulfide. The now low overall intensity of all of the peaks in the spectrum indicates a nearly

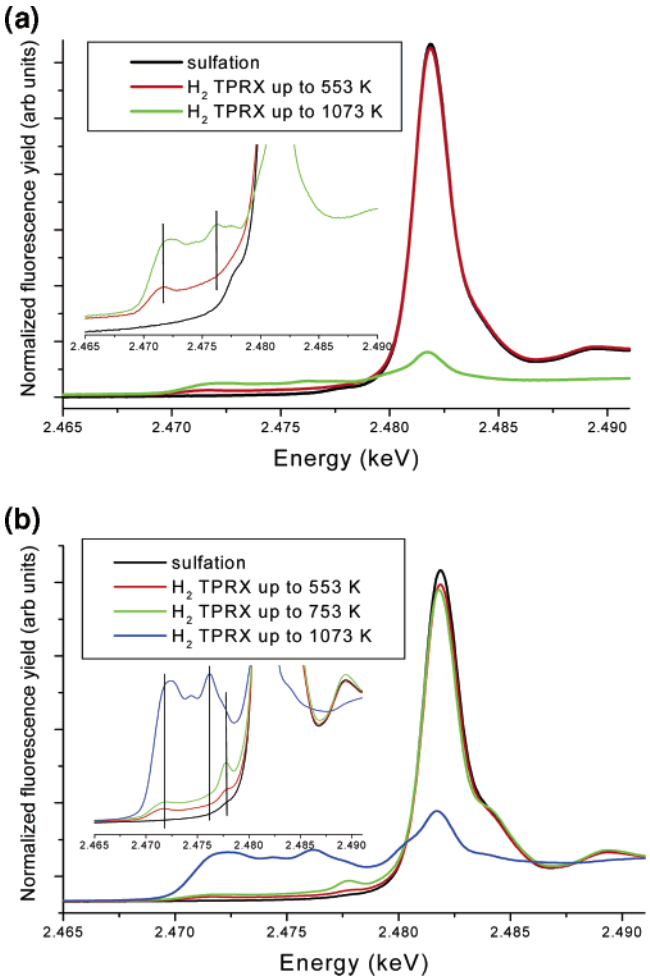

Figure 3. Sulfur K-edge XANES spectra of (a) 5 g/L Pt-BaO(8)/Al_2O_3 and (b) 5 g/L Pt-BaO(20)/Al_2O_3 samples.

complete removal of sulfur from this sample, presumably via the formation of gas-phase H_2S observed in the H_2 TPRX data.

The Pt-BaO(20)/Al_2O_3 sample shows qualitatively similar behavior as illustrated in Figure 3b. Up to 743 K, the dominant sulfate species are stable as evidenced by the very small drop in intensity for the 2482 eV peak, although small sulfide and sulfite peaks are observed as for the Pt-BaO(8)/Al_2O_3 sample. The spectrum for the Pt-BaO(20)/Al_2O_3 sample obtained after H_2 TPRX up to 1073 K (Figure 3b, blue curve) consists of a number of broad peaks with maxima between 2742 and 2482 eV. Compared with the Pt-BaO(8)/Al_2O_3 sample, the Pt-BaO-(20)/Al_2O_3 one contains a significantly larger amount of residual sulfur species of all types after H_2 TPRX up to 1073 K; notably, significant intensity in the spectrum for sulfate species is still present for the Pt-BaO(20)/Al_2O_3 sample. This comparison is consistent with the H_2 TPRX results in that both sets of data indicate that removal of sulfur is significantly more complete for the Pt-BaO(8)/Al_2O_3 sample than for Pt-BaO(20)/Al_2O_3. Thus, we conclude that the lower loading of barium in Pt-BaO/Al_2O_3 LNT materials enables more facile desulfation by H_2.

We have shown that in situ TR-XRD is an excellent technique for following the phase changes of $Ba(NO_3)_2/Al_2O_3$ during NOx adsorption, reaction, and desorption.[7] Moreover, the TR-XRD experiment can be operated under conditions of increasing temperature with H_2 flowing that are essentially identical with those of H_2 TPRX, thus providing complementary information about the phase changes for the Pt-BaO/Al_2O_3 samples studied here.

A series of TR-XRD patterns obtained for the 10 g/L sulfated Pt-BaO(20)/Al_2O_3 during H_2 reduction in the 300−1073 K temperature range is shown in Figure 4a. The room temperature XRD pattern contains peaks at 11.28° and 15.39° arising from $Ba(NO_3)_2$ (JCPDS 24-0053) and $BaSO_4$ (JCPDS 05-0448), respectively. $Ba(NO_3)_2$ species remain due to the incomplete calcinations at 773 K, which is not high enough to decompose all the $Ba(NO_3)_2$ species prior to sulfation. However, the intensities of the diffraction peaks due to the $Ba(NO_3)_2$ phase are negligible compared with those of an as-prepared sample.[7] Thus, we believe that most of the barium species are available to form $BaSO_4$ during sulfation. Up to about 773 K, the XRD patterns are unchanged except for the disappearance of the peaks due to $Ba(NO_3)_2$, suggesting that the $BaSO_4$ phases are stable. Above 773 K, diffraction peaks associated with a new BaS phase at 16.60° (JCPDS 08-0454) appear and continue to grow with increasing temperature, along with a corresponding drop in the intensities of the $BaSO_4$ peaks. The variation of the integrated intensities of the $BaSO_4$ (210) and BaS (200) diffraction peaks and the crystalline sizes of the $BaSO_4$ and BaS phases calculated from the fwhm of main peaks is plotted in Figure 4, parts b and c, respectively. The results shown in these figures clearly demonstrate that a transformation of at least a portion of $BaSO_4$ to BaS occurs around 773 K, in the same temperature range in which significant H_2S begins to appear in the TPRX data (Figure 1). It is perhaps significant that diffraction peaks due to a PtS phase are not observed during hydrogen treatment up to 1073 K. Notably, Amberntsson et al.[28] have suggested that sulfur species exist as PtS during rich cycles when sulfur is present. A possible reason for this discrepancy is that the crystalline sizes of PtS are too small to be detected by XRD in our experiments. However, we clearly show that large crystalline particles of BaS are formed under reducing conditions above 773 K.

Figure 5a shows a series of XRD patterns during H_2 TPRX for the 5 g/L Pt-BaO(20)/Al_2O_3 sample. We observed similar phase transformation behavior to that of the 10 g/L sulfated Pt-BaO(20)/Al_2O_3 sample. Furthermore, with reference to Figures 1 and 3, it is clear that these results are in good agreement with H_2 TPRX and sulfur XANES that the dominant sulfate species are not changing until 773 K. The diffraction peak analysis of the phases, as displayed in Figure 5b,c, shows that the peak areas of the $BaSO_4$ and BaS phases in the 5 g/L sulfated sample are about 30% less than those in the 10 g/L one. However, the estimated particle sizes are roughly comparable.

Changes in the XRD patterns upon H_2 TPRX for the 5 g/L sulfated Pt-BaO(8)/Al_2O_3 sample are displayed in Figure 6a. It should be noted that a $BaCO_3$ phase (JCPDS 05-0378) is present because this sample was initially prepared more than six months prior to use for these studies, and an additional calcination at 773 K before sulfation is not sufficiently high enough to decompose all the $BaCO_3$ species that formed during storage. However, we have previously shown that the existence of a minority $BaCO_3$ phase did not influence the interpretation of the NOx adsorption/release chemisty.[7] As with the sulfated Pt-BaO(20)/Al_2O_3 samples, the temperature range in which sulfate diffraction peaks disappear and BaS peaks appear for Pt-BaO-(8)/Al_2O_3 is consistent with the H_2 TPRX and sulfur XANES data discussed above. In Figure 6b,c, the changes in the integrated peak intensity of the (210) $BaSO_4$ and (200) BaS diffraction features and their average particle size estimated from the fwhm of these primary peaks during the TPRX are displayed. Comparing these results with those for the 5 g/L sulfated Pt-

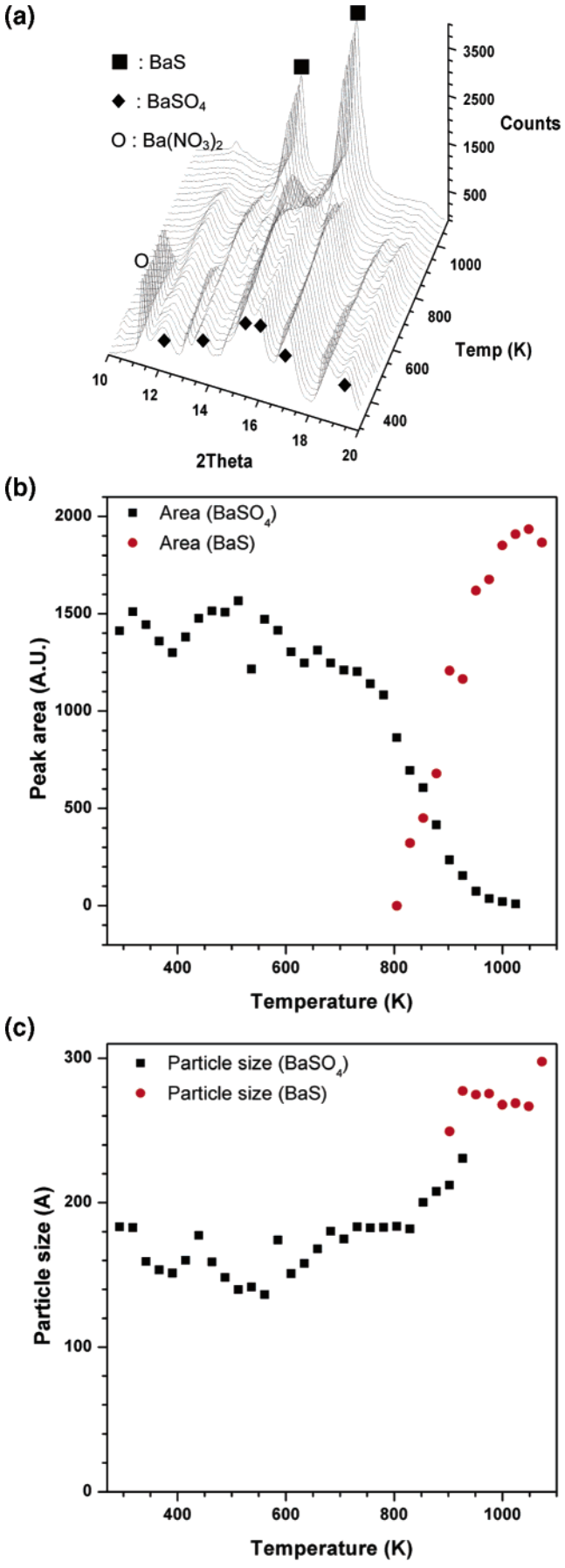

Figure 4. (a) TR-XRD patterns collected during H_2 TPRX from a 10 g/L Pt-BaO(20)/Al_2O_3 sample. (b) Integrated area of the diffraction peak and (c) the calculated average particle size of $BaSO_4$ and BaS as a function of sample temperature.

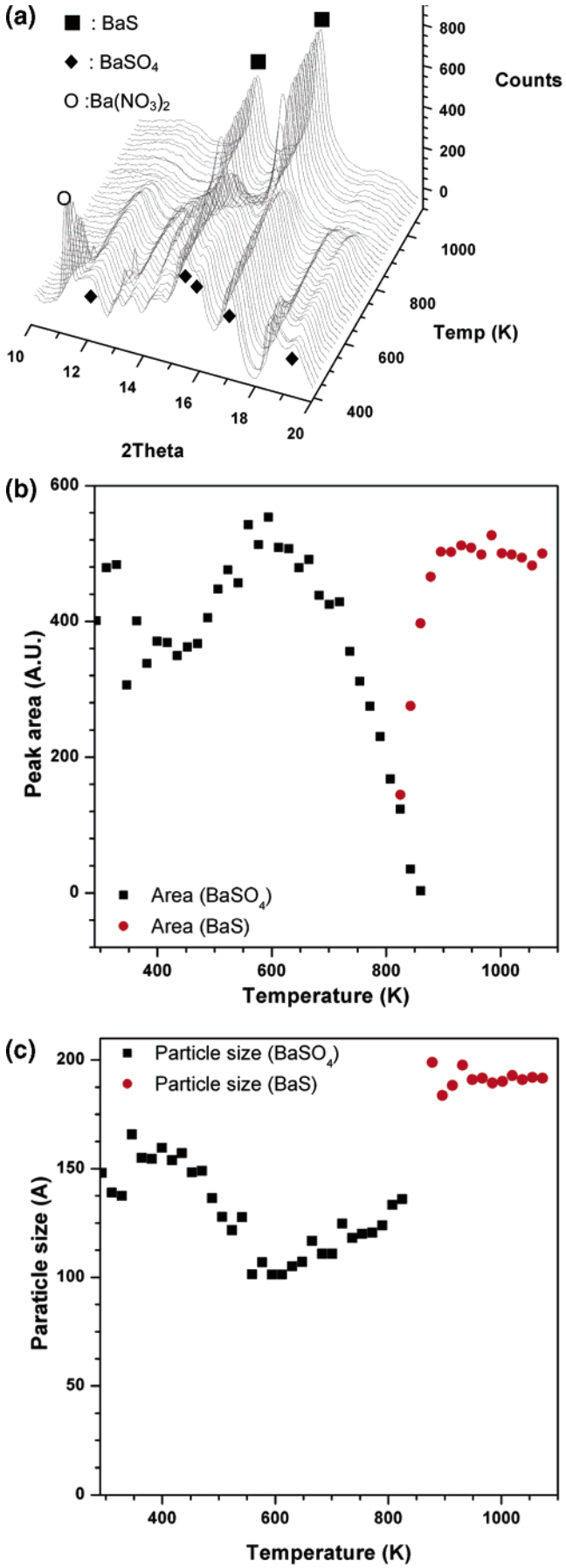

Figure 5. (a) TR-XRD patterns collected during H_2 TPRX from a 5 g/L Pt-BaO(20)/Al_2O_3 sample. (b) Integrated area of the diffraction peak and (c) the average particle size of $BaSO_4$ and BaS as a function of sample temperature.

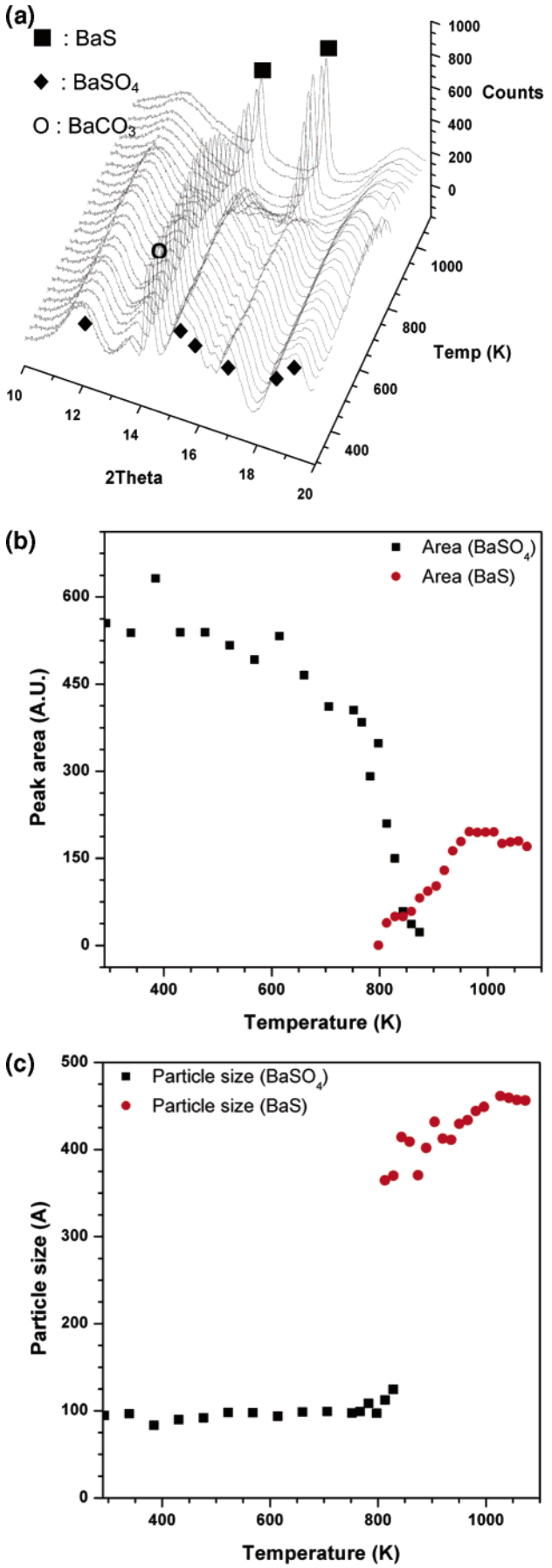

Figure 6. (a) TR-XRD patterns collected during H_2 TPRX from a 5 g/L Pt-BaO(8)/Al_2O_3 sample. (b) Integrated area of the diffraction peak and (c) the average particle size of $BaSO_4$ and BaS as a function of sample temperature.

BaO(20)/Al_2O_3 sample (Figure 5b,c), the peak area of $BaSO_4$ in Pt-BaO(8)/Al_2O_3 is almost the same, although the peak area of the BaS phase is significantly smaller for the lower Ba-loaded sample. This result agrees well with the sulfur XANES spectra after H_2 TPRX up to 1073 K, which also indicated that residual sulfur species were present at much lower concentrations for the Pt-BaO(8)/Al_2O_3 sample. However, the average particle size of the BaS phase in Pt-BaO(8)/Al_2O_3 is actually as much as two times larger than that in Pt-BaO(20)/Al_2O_3 despite its smaller peak area. Also of note is that the average particle size of unreduced $BaSO_4$ phases, about 10 nm, is actually significantly smaller than those in the sulfated Pt-BaO(20)/Al_2O_3 sample, perhaps as a result of the fact that they originate from the surface type BaO/$BaCO_3$ species in the fresh Pt-BaO(8)/Al_2O_3 sample. Again, the aggregate of these results indicate that the desulfation processes depend on the barium loading, likely because of differing morphologies for the various Ba phases present.

The changing morphology of the Pt-BaO(8)/Al_2O_3 and Pt−BaO(20)/Al_2O_3 system upon 5 g/L sulfation and desulfation with H_2 up to 1073 K was also investigated by TEM, and EDS was used to determine the sample composition. TEM images from the 5 g/L sulfated Pt-BaO(8)/Al_2O_3 and Pt-BaO(20)/Al_2O_3 samples are shown in Figure 7, parts a and b, respectively. Both samples contain identifiable dark areas on the light-colored alumina support material. However, the EDS results (shown as insets in the figures) for two selected regions of the particles suggest that light and dark areas of both samples contain a relatively constant ratio of Ba, Al, and S. Also, we note that crystalline $BaSO_4$ particles cannot be distinguished in the TEM images of either Pt-BaO/Al_2O_3 samples. In other words, the contrast difference is more likely arising from the sample thickness, not from heterogeneity of the samples. On the other hand, in the case of the desulfated samples as shown in Figure 8a,b, there is a drastic change in the composition depending on the analyzed region of the sample. For example, one dark spot in Figure 8a is rich in both barium and sulfur, while other regions are aluminum rich suggesting that some dark spots contain significant quantities of a BaS phase. This BaS "segregation" is even more pronounced in the Pt-BaO(20)/Al_2O_3 sample as shown in Figure 8b. Although the particle size of BaS in Figure 8a looks smaller than that in Figure 8b, we do not believe that the TEM results conflict with the XRD results described above because the local information from TEM cannot represent the sample-average data obtained with XRD. Furthermore, it is often very difficult to accurately determine the size of BaS particles of the desulfated samples in the TEM images. Finally, it is notable that the EDS concentrations for sulfur in the 5 g/L desulfated Pt-BaO(20)/Al_2O_3 sample are considerably higher than the Pt-BaO(8)/Al_2O_3 one, fully consistent with the H_2 TRPX and S XANES results.

4. Discussion

We have shown that Pt-BaO/Al_2O_3 samples form SO_4^{2-} species during sulfation at 573 K independent of barium loading. In the Pt-BaO(8)/Al_2O_3 sample, the barium loading is below that necessary to completely cover the alumina surface (<1 monolayer). In this case, sulfates appear to form on exposed alumina surfaces as well as on the Ba phases present. The total amount of SO_2 uptake increases with the amount of barium for the same level of sulfation (Table 1). This implies that any sulfate species formed on bare alumina would remain on the Al_2O_3 surface. In this regard, note also the absence of evidence for an $Al_2(SO_4)_3$ phase in the XRD data. We have previously

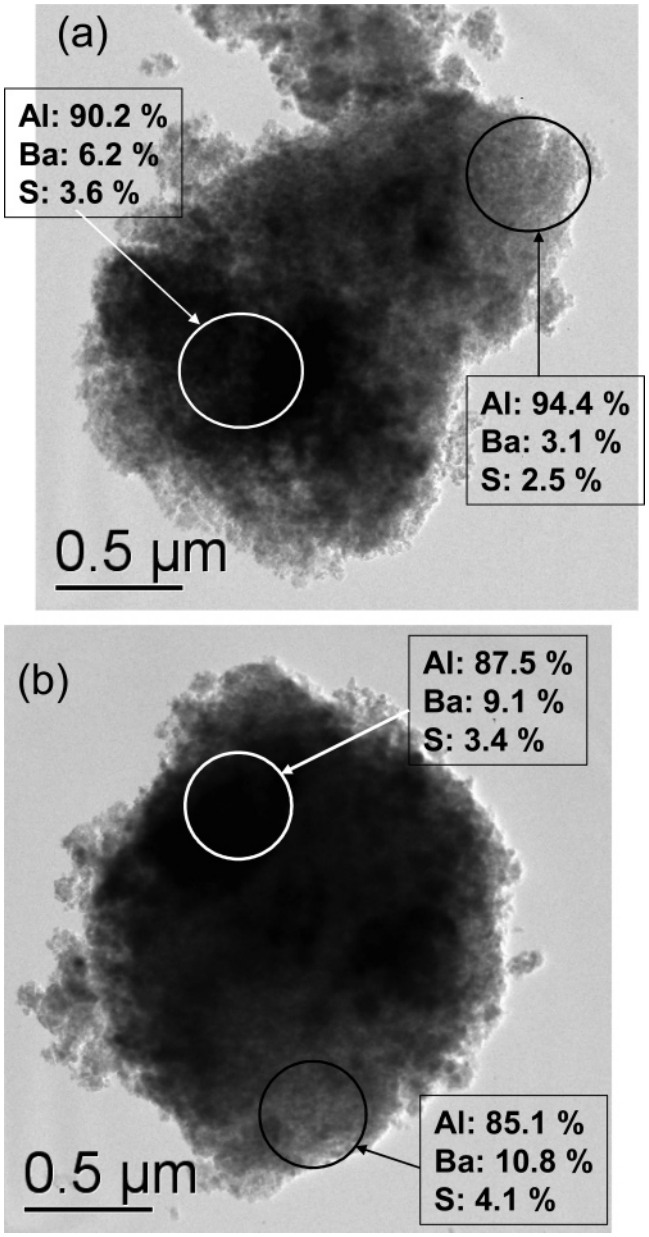

Figure 7. TEM images of (a) sulfated 5 g/L Pt-BaO(8)/Al_2O_3 and (b) sulfated 5 g/L Pt-BaO(20)/Al_2O_3 samples. Circles indicate the results of the EDS from selected spots.

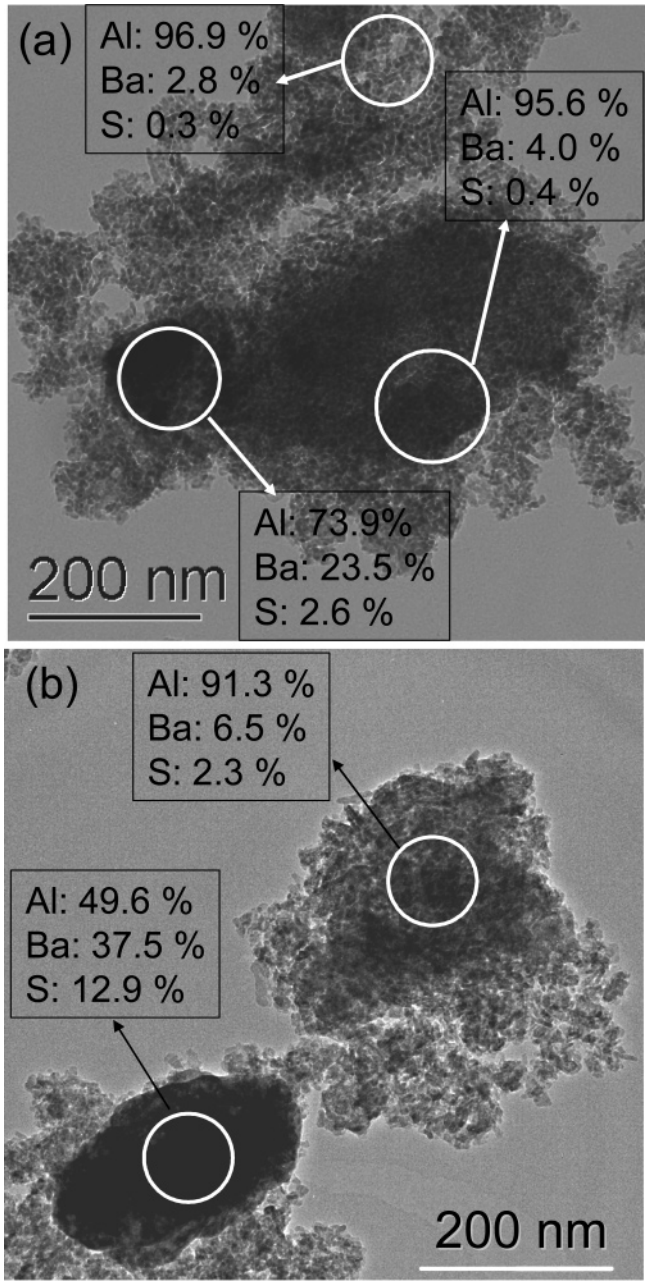

Figure 8. TEM images of (a) desulfated 5 g/L Pt-BaO(8)/Al_2O_3 and (b) desulfated 5 g/L Pt-BaO(20)/Al_2O_3 samples. Circles indicate the results of the EDS from selected spots.

shown that the Ba phase in the Pt-BaO(8)/Al_2O_3 sample uniformly coats the alumina surface.[7] During the sulfation, essentially all these "monolayer" BaO/$BaCO_3$ species will be available to form $BaSO_4$ until saturation. In contrast, some of the bulk BaO/$BaCO_3$ particles present in the Pt-BaO(20)/Al_2O_3 sample will not be converted to sulfates even after large SO_2 exposures. This is almost certainly due to diffusion limitations on the formation of barium sulfate into the large particles, analogous to limitations on $Ba(NO_3)_2$ formation on large Ba-containing particles during NOx uptake as suggested by Olson et al.[20] Furthermore, the TEM/EDS results indicate a largely homogeneous distribution of sulfur without significant morphology changes to the Pt-BaO/Al_2O_3 samples upon sulfation.

While differences between the Pt-BaO(8)/Al_2O_3 and Pt-BaO(20)/Al_2O_3 samples during SO_2 uptake at 573 K were relatively small, dramatic differences were observed during the desulfation process carried out at higher temperatures in a H_2-containing flow. The Pt-BaO(8)/Al_2O_3 sample is desulfated via the formation of a larger amount of H_2S despite the fact that it had lower initial levels of sulfur after sulfation. Importantly, desulfation also occurred at lower temperatures for this sample. Thus, the Pt-BaO(8)/Al_2O_3 sample contains much lower amounts of sulfur species remaining than Pt-BaO(20)/Al_2O_3. As with SO_2 uptake, the initial morphology differences between these two samples likely plays a role in determining the extent of desulfation and the temperature at which it occurs. Indeed, the TR-XRD data indicated that the average size of the $BaSO_4$ particles was significantly smaller for the sulfated Pt-BaO(8)/Al_2O_3 sample. This result coupled with the TEM/EDS data suggest that the initial "monolayer" morphology for the Ba phase in the Pt-BaO(8)/Al_2O_3 sample is largely maintained upon sulfation. Thus, desulfation may occur to a greater extent and at lower temperatures because it does not require the removal of sulfur from the interior of large bulk particles of $BaSO_4$ as in the case for the Pt-BaO(20)/Al_2O_3 sample. We could also speculate that the presence of Ba−O−Al bonds in a "monolayer" morphology

may modify, in a positive way (i.e., weaken), the Ba−S bonds in a resultant sulfate phase. The suggestion that a "monolayer"-type barium sulfate phase may provide for more facile (i.e., lower temperature) and more complete desulfation than bulk barium sulfates is potentially important with respect to the improvement of the LNT technology.

During the desulfation process at temperatures higher than 773 K, a new BaS phase is observed for both samples regardless of the barium loading. Interestingly, while considerably fewer in number, the average crystallite size of the BaS phase in Pt-BaO(8)/Al_2O_3 is estimated to be much larger than that of Pt-BaO(20)/Al_2O_3 after H_2 TPRX up to 1073 K. Although the reasons for this behavior are not clear to us, it does suggest that the Pt-BaO(8)/Al_2O_3 sample may perhaps be more prone to deactivation to multiple sulfation/desulfation cycles. This possibility is currently being explored via a study of the NOx adsorption/desorption process in the presence of SO_2 for samples with various barium loadings, and including periodic desulfation events.

5. Conclusion

The effect of barium loading on desulfation processes for sulfated Pt-BaO/Al_2O_3 samples was investigated by using H_2 TPRX, sulfur XANES, in situ XRD, and TEM/EDS techniques. We prepared the Pt-BaO(8)/Al_2O_3 and Pt-BaO(20)/Al_2O_3 samples as representative of materials that initially contain predominantly "monolayer" and bulk Ba phases, respectively. As such, we find that some of the barium species in Pt-BaO(20)/Al_2O_3 are inaccessible to the SO_2 adsorption because of diffusion limitations in the formation of sulfate species into the interior region of the particulate Ba phase. Surface barium sulfates, originally from the "monolayer" BaO/$BaCO_3$ phase in Pt-BaO(8)/Al_2O_3, were more readily (i.e., at lower temperature) and completely removed as gaseous H_2S than the bulk sulfates in Pt-BaO(20)/Al_2O_3 during the H_2 TPRX. After high temperature desulfation for both samples, residual sulfur exists in a reduced form, primarily as fairly large BaS particles. We conclude that the lower barium loadings provide for more optimum conditions for the removal of sulfur and, correspondingly, reduced deactivating effects.

Acknowledgment. The authors would like to thank Dr. Wolfgang Caliebe and Dr. Katrina Pearison for help with the Sulfur K-edge XANES spectroscopy measurements at the National Synchrotron Light Source (NSLS). Financial support was provided by the U.S. Department of Energy (DOE), Office of Freedom Car and Vehicle Technologies. The work was performed in the Environmental Molecular Sciences Laboratory (EMSL) at the Pacific Northwest National Laboratory (PNNL). The EMSL is a national scientific user facility supported by the U.S. DOE Office of Biological and Environmental Research. PNNL is a multiprogram national laboratory operated for the U.S. Department of Energy by Battelle Memorial Institute under Contract DE-AC06-76RLO 1830. The work at Brookhaven National Laboratory was financed through Contract DE-AC02-98CH10086 with the DOE (Division of Chemical Sciences).

References and Notes

(1) Epling, W. S.; Campbell, L. E.; Yezerets, A.; Currier, N. W.; Parks, J. E. *Catal. Rev. Sci. Eng.* **2004**, *46*, 163.
(2) Takahashi, N.; Shinjoh, H.; Iijima, T.; Suzuki, T.; Yamazaki, K.; Yokota, K.; Suzuki, H.; Miyoshi, N.; Matsumoto, S.; Tanizawa, T.; Tanaka, T.; Tateishi, S.; Kasahara, K. *Catal. Today* **1996**, *27*, 63.
(3) Fridell, E.; Persson, H.; Westerberg, B.; Olsson, L.; Skoglundh, M. *Catal. Lett.* **2000**, *66*, 71.
(4) Fridell, E.; Skoglundh, M.; Westerberg, B.; Johansson, S.; Smedler, G. *J. Catal.* **1999**, *183*, 196.
(5) Prinetto, F.; Ghiotti, G.; Nova, I.; Lietti, L.; Tronconi, E.; Forzatti, P. *J. Phys. Chem.* B **2001**, *105*, 12732.
(6) Szanyi, J.; Kwak, J. H.; Kim, D. H.; Burton, S. D.; Peden, C. H. F. *J. Phys. Chem. B* **2005**, *109*, 27.
(7) Szanyi, J.; Kwak, J. H.; Hanson, J.; Wang, C. M.; Szailer, T.; Peden, C. H. F. *J. Phys. Chem. B* **2005**, *109*, 7339.
(8) Olsson, L.; Persson, H.; Fridell, E.; Skoglundh, M.; Andersson, B. *J. Phys. Chem. B* **2001**, *105*, 6895.
(9) Lietti, L.; Forzatti, P.; Nova, I.; Tronconi, E. *J. Catal.* **2001**, *204*, 175.
(10) Nova, I.; Castoldi, L.; Lietti, L.; Tronconi, E.; Forzatti, P. *Catal. Today* **2002**, *75*, 431.
(11) Olsson, L.; Fridell, E. *J. Catal.* **2002**, *210*, 340.
(12) Engstrom, P.; Amberntsson, A.; Skoglundh, M.; Fridell, E.; Smedler, G. *Appl. Catal., B* **1999**, *22*, L241.
(13) Liu, Z. Q.; Anderson, J. A. *J. Catal.* **2004**, *228*, 243.
(14) Su, Y.; Amiridis, M. D. *Catal. Today* **2004**, *96*, 31.
(15) Sedlmair, C.; Seshan, K.; Jentys, A.; Lercher, J. A. *Catal. Today* **2002**, *75*, 413.
(16) Elbourazzaoui, S.; Corbos, E. C.; Courtois, X.; Marecot, P.; Duprez, D. *Appl. Catal., B* **2005**, *61*, 236.
(17) Wei, X. Y.; Liu, X. S.; Deeba, M. *Appl. Catal., B* **2005**, *58*, 41.
(18) Szailer, T.; Kwak, J. H.; Kim, D. H.; Szanyi, J.; Wang, C. M.; Peden, C. H. F. *Catal. Today*. **2006**, *114*, 86.
(19) Wang, X. Q.; Hanson, J. C.; Frenkel, A. I.; Kim, J. Y.; Rodriguez, J. A. *J. Phys. Chem. B* **2004**, *108*, 13667.
(20) Olsson, L.; Blint, R. J.; Fridell, E. *Ind. Eng. Chem. Res.* **2005**, *44*, 3021.
(21) Huffman, G. P.; Shah, N.; Huggins, F. E.; Stock, L. M.; Chatterjee, K.; Kilbane, J. J.; Chou, M. I. M.; Buchanan, D. H. *Fuel* **1995**, *74*, 549.
(22) Rodriguez, J. A.; Jirsak, T.; Perez, M.; Chaturvedi, S.; Kuhn, M.; Gonzalez, L.; Maiti, A. *J. Am. Chem. Soc.* **2000**, *122*, 12362.
(23) Solomon, D.; Lehmann, J.; Martinez, C. E. *Soil Scie. Soc. Am. J.* **2003**, *67*, 1721.
(24) Rodriguez, J. A.; Chaturvedi, S.; Hanson, J. C.; Brito, J. L. *J. Phys. Chem. B* **1999**, *103*, 770.
(25) Rodriguez, J. A.; Jirsak, T.; Freitag, A.; Hanson, J. C.; Larese, J. Z.; Chaturvedi, S. *Catal. Lett.* **1999**, *62*, 113.
(26) Song, I. H.; Rickett, B.; Janavicius, P.; Payer, J. H.; Antonio, M. R. *Nucl. Instrum. Methods Phys. Res., Sect. A* **1995**, *360*, 634.
(27) Huffman, G. P.; Mitra, S.; Huggins, F. E.; Shah, N.; Vaidya, S.; Lu, F. L. *Energy Fuels* **1991**, *5*, 574.
(28) Amberntsson, A.; Skoglundh, M.; Ljungstrom, S.; Fridell, E. *J. Catal.* **2003**, *217*, 253.